Heat Transfer Research 51(3):217–232 (2020)

HEAT TRANSFER IN MAGNETITE (Fe_3O_4) NANOPARTICLES SUSPENDED IN CONVENTIONAL FLUIDS: REFRIGERANT-134A ($C_2H_2F_4$), KEROSENE ($C_{10}H_{22}$), AND WATER (H_2O) UNDER THE IMPACT OF DIPOLE

A. Majeed,[1] A. Zeeshan,[2] M.M. Bhatti,[3,4,] & R. Ellahi[2,5]*

[1]*Department of Mathematics and Statistics, Bacha Khan University Charsadda, kpk, Pakistan*

[2]*Department of Mathematics and Statistics, FBAS, IIUI, Islamabad, Pakistan*

[3]*College of Mathematics and Systems Science, Shandong University of Science and Technology, Qingdao, Shandong, 266590, China*

[4]*Shanghai Institute of Applied Mathematics and Mechanics, Shanghai University Yanchang Road, Shanghai 200072, China*

[5]*Center for Modeling & Computer Simulation, Research Institute, King Fahd University of Petroleum & Minerals, Dhahran, Saudi Arabia*

*Address all correspondence to: M.M. Bhatti, College of Mathematics and Systems Science, Shandong University of Science and Technology, Qingdao, Shandong, 266590, China, Shanghai Institute of Applied Mathematics and Mechanics, Shanghai University Yanchang Road, Shanghai 200072, China, E-mail: mubashirme@yahoo.com

Original Manuscript Submitted: 1/8/2019; Final Draft Received: 6/28/2019

In this article, theoretical investigation has been performed to explore the heat transport characteristics of a magnetic nanofluid (ferrofluid) with dipole field impact. We considered magnetite (Fe_3O_4) nanoparticles suspended in three base fluids such as kerosene ($C_{10}H_{22}$), Refrigerant-134a ($C_2H_2F_4$), and water (H_2O). Magnetic dipole is of importance as it controls the momentum and thermal boundary layer region. Also characterization of magnetothermomechanical (ferrohydrodynamic) interaction decelerates the motion of the fluid as compared to the hydrodynamic case. Governing flow problem is normalized into ordinary differential equation by adopting the similarity transform procedure and thereafter solving by an effective shooting algorithm. Flow is generated due to a linearly porous stretched surface. Impact of involved constraints, namely, ferromagnetic parameter, suction, porosity, slip, and volume concentration of nanoparticle on friction factor and heat transfer rate are explained by graphs and tables. From the results we infer that the influence of ferrohydrodynamics is to flatten the velocity profile, whereas the decreasing effect is seen for the temperature profile for large values of nanoparticle volume fraction. Also it is shown that the Nusselt number is higher for the case of Refrigerant-134a for large values of concentration of nanoparticles.

KEY WORDS: *heat transfer, ferrofluid, boundary layer flow, magnetite (Fe_3O_4), porous media, partial slip*

1. INTRODUCTION

Study of heat transport in nanofluid flow is of prime importance in the present research works. It has remarkable application in solving industrial and engineering problems of microelectronics, chemical production, microfluidics, transportation, nuclear reactors, and domestic refrigerators. The vision of nanofluid was first introduced by Choi (1965). Nanofluids are innovative and smart fluids including micron-sized particles suspended in a carrier fluid

NOMENCLATURE

a	distance of permanent point in vertical direction
c_p	specific heat transfer, $J \cdot kg^{-1} \cdot K^{-1}$
C_{fx}	skin friction coefficient
H	magnetic field, A/m
k	thermal conductivity, $W \cdot m^{-1} \cdot K^{-1}$
K_1	porosity parameter
K^*	pyromagnetic coefficient
l	characteristic length
M	magnetization, A/m
Nu_x	local Nusselt number
Pr	Prandtl number
Re_x	Reynolds number
S	suction/injection parameter
T	fluid temperature
T_c	Curie temperature, K
u, v	velocity components, $m \cdot s^{-1}$
x, y	Cartesian coordinates, m

Greek Symbols

α	thermal diffusivity
α_1	dimensionless distance from the origin to the magnetic dipole
β	ferromagnetic interaction parameter
γ	strength of magnetic field, A/m
ε	dimensionless Curie temperature
ρ	density, $kg \cdot m^{-3}$
ρc_p	heat capacity
Φ	magnetic potential
ψ	stream function, $m^2 \cdot s^{-1}$
δ	velocity slip parameter
ϕ	volume concentration of nanoparticles
τ	shear stress
λ	dissipation parameter
μ_o	magnetic permeability
μ	viscosity

Subscripts

f	fluid
nf	nanofluid
s	solid particle
w	wall

of diameter of about 10 nm. The thermal conductivity of conventional fluids such as ethylene glycol and water is small in comparison with crystalline solids, although the inclusion of the lowest quantity of solid particles demonstrates a drastic change in the enhancement of thermal conductivity (Choi et al., 2004). Nanofluids involving metallic or ceramic nanoparticles exhibited massive enlargement in thermal conductivity that cannot be described by outdated studies (Lee et al., 1999). Heat transfer augmentation and thermal conductivity enhancement in a conventional fluid was performed by Yu et al. (2008). They showed that increment during heat transport can be calculated in the range from 15% to 40%. Masuda et al. (1993) revealed the importance of heat conduction enhancement and viscosity of fluid with the distributed ultrafine microparticles. Khan and Pop (2011) obtained similar results for free convective boundary layer flow of nanofluid over a flat plate under the influence of a porous medium. Yirga and Tesfay (2015) studied transfer of heat in a nanofluid under the influence of magnetic field through a porous medium. They revealed that a Cu–water-based nanofluid shows lower values of skin friction than the Ag–water one. Kumar and Elansezhian (2012) performed an experimental study of Al_2O_3–Refrigerant-134a-based nanofluid in a cooling system. They showed that heat transfer coefficient increases in the presence of nano-Al_2O_3 particles. Chamkha and Aly (2010) conveyed a magnetic impact on nanofluid flow toward an embedded vertical surface with heat generation and suction. Rahman et al. (2012) examined the influence of the dynamics of natural convection on water-based nanofluids with slip flow over a wedge with the occurrence of heat generation. Bhaskar et al. (2014) analyzed velocity slip effect and variable thermal conductivity on copper-based nanofluid flow due to a stretched surface. Rajesh et al. (2015) inspected nanofluid flow near a transient free convective porous plate under the influence of viscous dissipation and magnetic field by applying the Galerkin-based finite element technique. Reddy and Chamkha (2016) examined heat transfer and magnetohydrodynamic convective boundary layer flow of nanofluid via porous media with different sizes and shapes of nanoparticles.

Moreover, a ferrofluid is a special kind of liquid with magnetic nanoparticles. They are colloidal single-domain ferroparticles in a carrier liquid. Flow of ferrofluid and heat transfer could be controlled by external magnetic field. These fluid characteristics fascinated engineers and scientists, since the fluid has countless applications in biomedicine, purification of liquid, microelectromechanical systems (MEMS), metals, leak-proof seals, shock absorbers, lithographic patterning, and many others (Mamourian et al., 2016; Sheikholeslami and Ellahi, 2015; Ellahi et al., 2014, 2015; Nadeem et al., 2013; Mohyud-Din et al., 2015). Sheikholeslami and Ganji (2014) considered the impact of FHD and MHD on the free convective flow of ferrofluid in a semi-annular enclosure by employing CVFEM. Heat dissipation effects on a ferromagnetic fluid in a linearly heated cavity embedded with temperature profile was performed by Kefayati (2014). He expressed that with the rise of nanoparticle concentration, energy transport is reduced by using the LBM method. Sheikholeslami et al. (2015b) examined the effect of ferromagnetic particle on forced convective heat transfer on Fe_3O_4–water based nanofluid by applying the finite element procedure. They demonstrated that transfer of heat directly varies with Reynolds number and volume concentration of nanoparticles, whereas the reverse behavior is noted for the Hartmann number. Sheikholeslami and Rashidi (2015) characterized the influence of water-based magnetite (Fe_3O_4) nanofluid in a semi-annular enclosure. Sheikholeslami et al. (2015a) examined ferrofluid behavior and made an analysis of heat transport coupled with radiation impact under the mutual performance of FHD and MHD. Recently Majeed et al. (2019a) discussed the magnetic properties of nanoparticles due to applied magnetic dipole in an aqueous medium. Majeed et al. (2019b) performed the heat transfer analysis of MHD second-order slip flow with convective boundary condition and suction/injection. Some of the significant investigations on magnetic nanofluid flow, porous medium and slip can be seen in Hassan et al. (2018, 2019), Sheikholeslami et al. (2018, 2019), Zeeshan et al. (2018), Majeed et al. (2018, 2019c), Marin and Öchsner (2017), and Bhatti and Lu (2019).

Inspired by above-mentioned studies, the purpose of the present manuscript is to discover the impact of magnetite (Fe_3O_4) nanoparticle added to along dissimilar base fluids such as kerosene, water, and Refrigerant-134a under the effect of dipole field. The influence of convergence control parameters on the flow field such as ferrohydrodynamic parameter, slip, porosity, suction, and concentration of nanoparticles and on velocity, temperature, skin friction, and heat transfer rate are elaborated pictorially.

2. FERROHYDRODYNAMIC AND ENERGY FORMULATION

2.1 Problem Statement

We consider 2D viscous and electrically nonconducting incompressible ferromagnetic fluid comprising magnetite (Fe_3O_4) nanoparticles with the use of three conventional fluids like Refrigerant-134a ($C_2H_2F_4$), water (H_2O), and kerosene ($C_{10}H_{22}$) on a stretchable surface with wall velocity $u_w = cx$ (see Fig. 1). A permanent point dipole is exactly on the y axis at a distance "a" from a horizontal surface. Owing to the point dipole, the external magnetic field applied along the x axis intensifies the strength of the magnetic field and saturates the ferromagnetic fluid,

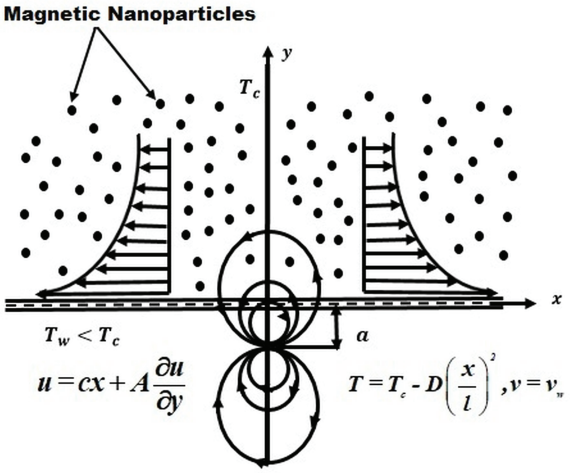

FIG. 1: Flow configuration in the problem

with T_w being the wall temperature and T_c being the Curie temperature. No further magnetization exists, when the ferromagnetic fluid reaches the Curie temperature.

The governing flow equations of ferrohydrodynamics and energy transport are (Tiwari and Das, 2007)

$$\frac{\partial u}{\partial x} + \frac{\partial v}{\partial y} = 0 , \tag{1}$$

$$u \frac{\partial u}{\partial x} + v \frac{\partial u}{\partial y} - \frac{\mu_0}{\rho_{nf}} M \frac{\partial H}{\partial x} = \frac{\mu_{nf}}{\rho_{nf}} \left(\frac{\partial^2 u}{\partial x^2} \right) - \frac{\mu_{nf}}{\rho_{nf} K} u , \tag{2}$$

$$\left(u \frac{\partial T}{\partial x} + v \frac{\partial T}{\partial y} \right) + \frac{\mu_0}{(\rho c_p)_{nf}} T \frac{\partial M}{\partial T} \left(u \frac{\partial H}{\partial x} + v \frac{\partial H}{\partial y} \right) = \alpha_{nf} \frac{\partial^2 T}{\partial y^2} + \frac{\mu_{nf}}{(\rho c_p)_{nf}} \left[\left(\frac{\partial u}{\partial y} \right)^2 + 2 \left(\frac{\partial v}{\partial y} \right)^2 \right] . \tag{3}$$

2.2 Boundary Conditions

The appropriate boundary conditions for the present study are

$$u = cx + A \frac{\partial u}{\partial y} , \quad T = T_c - D \left(\frac{x}{l} \right)^2 , \; v = v_w , \quad \text{at} \quad y = 0 , \tag{4}$$

$$T \to T_c , \; u \to 0, \quad \text{as} \; y \to \infty , \tag{5}$$

where x, y represent the Cartesian coordinates on the sheet and normal to it, u, v symbolize velocity components along the coordinate axis, μ_0 signifies the magnetic permeability, T is the fluid temperature, K is the permeability, and D and c are constants. The thermophysical constraints are as follows (Tiwari and Das, 2007):

$$\mu_{nf} = \frac{\mu_f}{(1-\phi)^{2.5}} , \quad \rho_{nf} = (1-\phi)\rho_f + \phi \rho_s , \tag{6}$$

$$\alpha_{nf} = \frac{k_{nf}}{(\rho c_p)_{nf}} , \quad (\rho c_p)_{nf} = (\rho c_p)_f (1-\phi) + (\rho c_p)\phi , \tag{7}$$

$$k_{nf} = k_f \left\{ \frac{k_s + 2k_f - 2\phi(k_f - k_s)}{k_s + 2k_f + \phi(k_f - k_s)} \right\} , \tag{8}$$

where ϕ is the volume concentration of nanoparticles, μ_f is the viscosity of the base fluid, ρ_f, ρ_s signify the densities of a pure fluid and nanoparticles, (k_f, k_s) characterize the thermal conductivities of the base fluid and nanoparticles, and k_{nf} is the thermal conductivity of the nanofluid.

2.3 Magnetic Dipole Field

Ferromagnetic fluid flow induced by a stretchable surface is exaggerated by the magnetic field because of the point dipole field. Such impact designated through magnetic scalar potential is defined as

$$\Phi = \frac{\gamma}{2\pi} \left(\frac{x}{x^2 + (y+a)^2} \right) . \tag{9}$$

Here γ represents the dipole moment per unit length. The quantities H_x and H_y are the magnetic components in the x and y directions specified by Andersson and Valnes (1998) as

$$H_x = -\frac{\partial \Phi}{\partial x} = \frac{\gamma}{2\pi}\left\{\left(\frac{x^2 - (y+a)^2}{\left(x^2 + (y+a)^2\right)^2}\right)\right\}, \tag{10}$$

$$H_y = -\frac{\partial \Phi}{\partial y} = \frac{\gamma}{2\pi}\left\{\left(\frac{2x\,(y+a)}{\left(x^2 + (y+a)^2\right)^2}\right)\right\}. \tag{11}$$

The strength of the magnetic body force corresponding to the gradient of the magnitude of H is defined in the following form:

$$H = \sqrt{\left(\frac{\partial \Phi}{\partial x}\right)^2 + \left(\frac{\partial \Phi}{\partial y}\right)^2}, \tag{12}$$

and

$$\frac{\partial H}{\partial x} = -\frac{\gamma}{2\pi}\left(\frac{2x}{(y+a)^4}\right), \quad \frac{\partial H}{\partial y} = \frac{\gamma}{2\pi}\left(\frac{-2}{(y+a)^3} + \frac{4x^2}{(y+a)^5}\right). \tag{13}$$

The impact of magnetization M can be expressed in the form of temperature by the linear expression given below:

$$M = K^*\left(T_c - T\right). \tag{14}$$

Here K^* signifies a pyromagnetic constant.

3. SIMILARITY TRANSFORMATION

We considered the following similarity variables suggested by Andersson and Valnes (1998)

$$\begin{aligned} \Psi(\xi, \eta) &= \left(\frac{\mu}{\rho}\right)\xi\, f(\eta), \\ \theta(\xi, \eta) &= \frac{T_c - T}{T_c - T_w} = \theta_1(\eta) + \xi^2\theta_2(\eta). \end{aligned} \tag{15}$$

Here $T_c - T_w = A\left(\frac{x}{l}\right)^2$ and the corresponding nondimensional variables are stated as

$$\xi = \sqrt{\frac{c}{\nu}}x, \qquad \eta = \sqrt{\frac{c}{\nu}}y. \tag{16}$$

The stream function is labeled in this way to justify the continuity equation directly, the components of velocity u, v are determined as follows:

$$\left.\begin{aligned} u &= \frac{\partial \Psi}{\partial y} = cxf'(\eta), \\ v &= -\frac{\partial \Psi}{\partial x} = -\sqrt{c\nu}f(\eta). \end{aligned}\right\} \tag{17}$$

By applying Eqs. (15)–(17) to Eqs. (2) and (3), we obtained the following coupled equations of the order of up to second order of ξ along with the boundary conditions (4) and (5):

$$f''' - (1-\phi)^{2.5}\left\{\left((1-\phi)+\phi\,\frac{\rho_s}{\rho_f}\right)\left(f'^2 - ff''\right)+\frac{2\beta\theta_1}{(\eta+\alpha_1)^4}\right\} - K_1 f' = 0\,, \tag{18}$$

$$\frac{k_{nf}}{k_f}\,\theta_1'' + \left[(1-\phi)+\phi\,\frac{(\rho c_p)_s}{(\rho c_p)_f}\right]\Pr(f\theta_1' - 2f'\theta) + \frac{2\lambda\beta\,(\theta_1-\varepsilon)\,f}{(\eta+\alpha_1)^3} - \frac{2\lambda}{(1-\phi)^{2.5}}\,f'^2 = 0\,, \tag{19}$$

$$\begin{aligned}\frac{k_{nf}}{k_f}\,\theta_2'' + \left[(1-\phi)+\phi\,\frac{(\rho c_p)_s}{(\rho c_p)_f}\right]\Pr\left(f\theta_2' - 4f'\theta_2\right) + \frac{2\lambda\beta\theta_2 f}{(\eta+\alpha_1)^3} - \lambda\beta\,(\theta_1-\varepsilon)\\ \times\left[\frac{2f'}{(\eta+\alpha_1)^4}+\frac{4f}{(\eta+\alpha_1)^5}\right] - \frac{\lambda}{(1-\phi)^{2.5}}\,f''^2 = 0\,,\end{aligned} \tag{20}$$

$$f' = 1+\delta f''\,,\quad f = S,\quad \theta_2 = 0,\quad \theta_1 = 1,\quad \text{at}\quad \eta = 0\,, \tag{21}$$

$$f' \to 0,\quad \theta_2 \to 0,\quad \theta_1 \to 0,\quad \text{as}\quad \eta \to \infty\,. \tag{22}$$

The pertinent parameters involved in the above system of nonlinear equations are defined as

$$\left.\begin{aligned}&\beta = \frac{\gamma\rho_f}{2\pi{\mu_f}^2}\,\mu_0 K^*\,(T_c - T_w)\,,\quad \lambda = \frac{c{\mu_f}^2}{\rho_f k\,(T_c - T_w)}\,,\quad K_1 = \frac{\nu_f}{cK}\,,\\ &S = \frac{-v_w}{\sqrt{c\nu_f}}\,,\ \Pr = \frac{(\mu c_p)_f}{k_f}\,,\quad \varepsilon = \frac{T_c}{T_c - T_w}\,,\ \alpha_1 = \sqrt{\frac{c\rho_f}{\mu_f}}a,\quad \delta = A\sqrt{\frac{c}{\nu_f}}\end{aligned}\right\}, \tag{23}$$

where β is the ferromagnetic parameter, λ is the viscous dissipation parameter, K_1 is the porosity parameter, S is the suction/injection parameter with $S > 0$ for suction and $S < 0$ for injection, Pr is the Prandtl number, α_1 is the dimensionless distance from the origin to the magnetic dipole, ε is the dimensionless Curie temperature ratio, and δ is the velocity slip parameter.

3.1 Skin Friction and Nusselt Number

From the practical point of view, the skin friction and Nusselt number are expressed as

$$C_{f_x} = \frac{-2\mu_{nf}\left(\dfrac{\partial u}{\partial y}\right)_{y=0}}{\rho_f\,(cx)^2}\,,\qquad \mathrm{Nu}_x = \frac{xk_{nf}\left(\dfrac{\partial T}{\partial y}\right)_{y=0}}{k_f\,(T_c - T_w)}\,. \tag{24}$$

By employing Eqs. (16)–(18), we get

$$C_f \mathrm{Re}_x^{1/2} = -\frac{2}{(1-\phi)^{2.5}}\,f''(0)\,,\qquad \mathrm{Nu}_x/\mathrm{Re}_x^{1/2} = -\frac{k_{nf}}{k_f}\left(\theta_1'(0) + \xi^2\theta_2'(0)\right). \tag{25}$$

Here $\mathrm{Re}_x = \dfrac{U_w x}{\nu}$ is the local Reynolds number, $f''(0)$ represents the wall shear stress (skin friction coefficient) and $(\theta_1'(0) + \xi^2\theta_2'(0))$ signifies the heat transfer coefficient (Nusselt number). It is more interesting and conve-

nient to replace the dimensionless wall heat transfer parameter by the dimensionless, and independent of the distance ξ, ratio $\theta^*(0) = \dfrac{\theta_1'(0)}{\theta_1'(0)\,|_{\beta=0}}$ called heat transfer rate at the wall.

4. NUMERICAL RESULTS AND DISCUSSION

Equations (18)–(20) with appropriate boundary equations (21) and (22) are coupled and nonlinear, which are very tough to tackle analytically, so we must solve them numerically by transforming them into an initial value problem by employing the Runga–Kutta technique using MATLAB software for some pertinent parameters which are defined in Eqs. (23) like the ferromagnetic interaction parameter β, volume concentration of nanoparticles ϕ, Prandtl number Pr, porosity parameter K_1, velocity slip parameter δ, and suction/injection parameter S formulated as

$$
\begin{aligned}
Z_1' &= Z_2,\\
Z_2' &= Z_3,\\
Z_3' &= (1-\phi)^{2.5}\left(\left[(1-\phi)+\phi\,\frac{\rho_s}{\rho_f}\right](Z_2^2 - Z_1Z_3) + \frac{2\beta Z_4}{(\eta+\alpha_1)^4}\right),\\
Z_4' &= Z_5,\\
Z_5' &= -\frac{k_n}{k_{nf}}\left(\mathrm{Pr}\left[(1-\phi)+\phi\,\frac{(\rho c_p)_s}{(\rho c_p)_f}\right](Z_1Z_5 - 2Z_2Z_4) + \frac{2\lambda\beta Z_1(Z_4-\varepsilon)}{(\eta+\alpha_1)^3} - \frac{2\lambda Z_2^2}{(1-\phi)^{2.5}}\right),\\
Z_6' &= Z_7,\\
Z_7' &= -\frac{k_{\mathrm{n}}}{k_{\mathrm{nf}}}\left(\mathrm{Pr}\left[(1-\phi)+\phi\,\frac{(\rho c_p)_{\mathrm{s}}}{(\rho c_p)_{\mathrm{f}}}\right](Z_1Z_7 - 4Z_2Z_6) + \frac{2\lambda\beta Z_1Z_6}{(\eta+\alpha_1)^3} - \lambda\beta(Z_4-\varepsilon)\left[\frac{2Z_2}{(\eta+\alpha_1)^4} + \frac{4Z_1}{(\eta+\alpha_1)^5}\right] - \frac{\lambda Z_3^2}{(1-\phi)^{2.5}}\right).
\end{aligned}
\tag{26}
$$

Here $Z_1 = f$, $Z_2 = f'$, $Z_3 = f''$, $Z_4 = \theta_1$, $Z_5 = \theta_1'$, $Z_6 = \theta_2$, $Z_7 = \theta_2'$; the corresponding initial conditions are $Z_1(0) = 0$, $Z_2(0) = 1 + \delta Z_3(0)$, $Z_3(0) = w_3$, $Z_4(0) = 1$, $Z_5(0) = w_5$, $Z_6(0) = 0$, and $Z_7(0) = w_7$. Here, w_3, w_5, and w_7 are proper guesses for $\theta_1'(0)$, $f''(0)$, and $\theta_2'(0)$ which are taken at $\eta_{\max} = 15$ to acquire good estimated solutions.

The obtained results for velocity and temperature distributions are drawn graphically in Figs. 1–7 for the set of numerous physical parameters like β, ϕ, Pr, K_1, δ, and S. Here we considered H_2O, $C_{10}H_{22}$, and $C_2H_2F_4$ as conventional base fluids and magnetite (Fe_3O_4) as solid nanoparticles thermal characteristics of which are displayed in Table 1. The fixed values in the entire study are taken as $\lambda = 0.01$, $\varepsilon = 2.0$, $\alpha_1 = 1.0$. To ensure the validity of the present numerical results, the calculated values of Nusselt number are compared with those obtained by Chen (1998), Abel et al. (2008), and Gireesha et al. (2014) and given in Table 2 for some values of Pr in the case of a pure fluid ($\phi = 0$) and good agreement is obtained. Computed results of skin friction and Nusselt number against the concentration of magnetite nanoparticles ϕ suspended in three base fluids—Refrigerant-134a ($C_2H_2F_4$), water (H_2O), and kerosene ($C_{10}H_{22}$)—are presented in Table 3 against the ferrohydrodynamic parameter β. It is observed that the values of skin friction and Nusselt number remain minimum without β and are greater in the presence of β. This is due to the alignment of magnetic solid nanoparticles in a definite order. It should also be noticed that the nanofluid based on Refrigerant-134a has a higher friction factor and heat transfer rate than the others.

The influence of volume concentration $0 \le \phi \le 2$ on flow fields in magnetite (Fe_3O_4) solid nanoparticles along with dissimilar conventional fluids, namely, kerosene ($C_{10}H_{22}$), Refrigerant-134a ($C_2H_2F_4$), and water (H_2O) are displayed graphically. It is interesting to observe in Fig. 2 that an increase in the volume concentration of nanoparticles reduces the velocity field and contradictory behavior is noted for the temperature field. Figure 2b shows the physical response demonstrated by the variation of nanoparticle concentration that illustrates the enhancement in thermal conductivity with associated boundary layer thickness. Further, Fig. 2a depicts that mag-

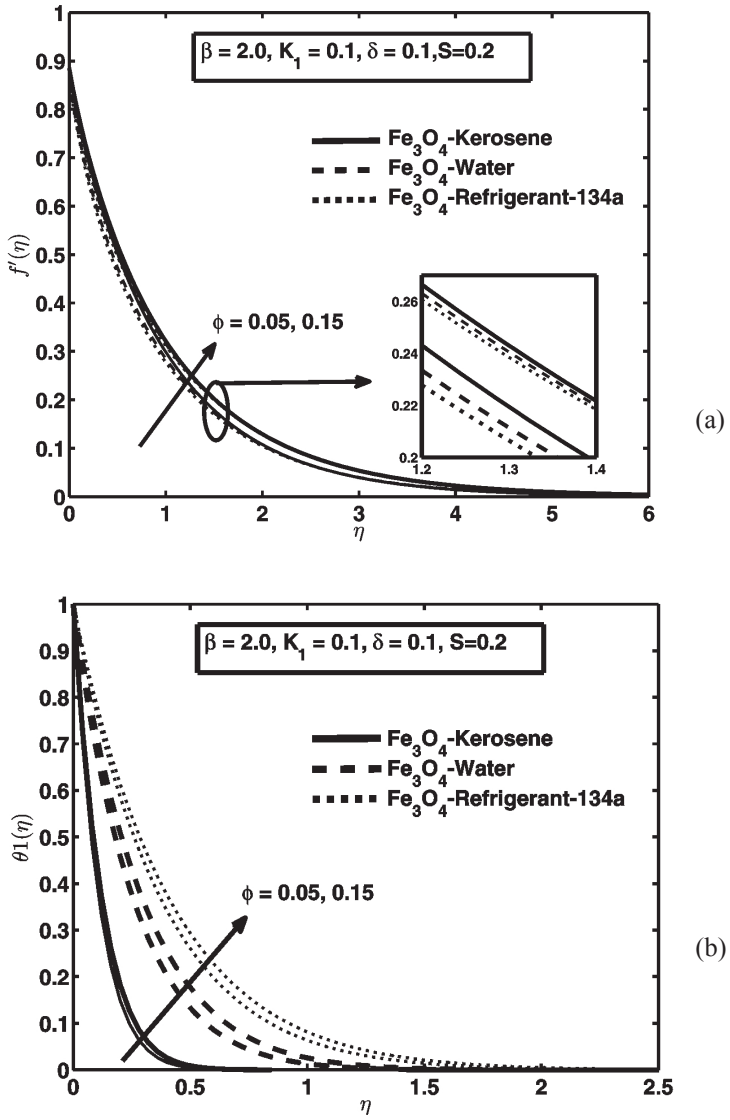

FIG. 2: (a) Sketch of ϕ on f', (b) sketch of ϕ on θ_1

netite (Fe_3O_4) solid nanoparticles with kerosene as a base fluid have a greater influence on the velocity field as associated to others, and gain highest improvement in temperature field for the Fe_3O_4–Refrigerant-134a nanofluid trailed by water and kerosene as shown in Fig. 2b.

Figure 3 represents the formation of velocity and temperature profiles for some values of the porosity parameter K_1 = 0.0, 0.4, and 0.8. From the given figure it is clear that velocity decays at higher porosity. This is obvious due to the increment in the permeability parameter, amplifying the resistance of porous media, which is responsible for the sluggish fluid motion, and a reverse impact is observed against the temperature field as exposed in Fig. 3b. Additionally, fluid velocity and corresponding boundary layer thickness increase in magnetite (Fe_3O_4) solid nanoparticles suspended in kerosene rather than in Refrigerant-134a and water, on the other hand, the temperature profile attains the highest value for the Fe_3O_4–Refrigerant-134a case as compared with other fluids.

Figure 4 describes the variation of velocity and temperature distributions under the impact of the slip parameter δ = 0.0, 0.4, and 0.8. Figure 4a discloses that wall velocity decreases at higher values of slip parameter and

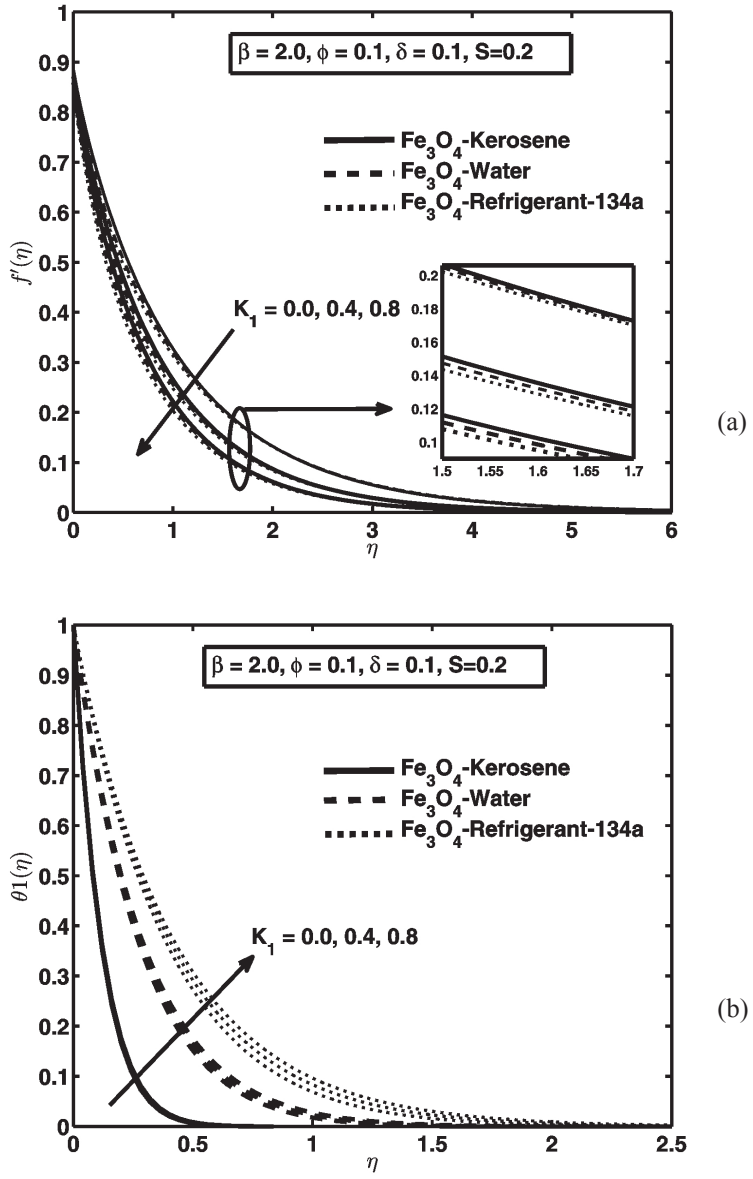

FIG. 3: (a) Sketch of K_1 on f', (b) sketch of K_1 on θ_1

approaches zero at η = 5. For the case of no-slip (δ = 0), velocity is equal to one. This is due to the fact that a larger value of δ increases the lubrication and slippage of the surface. Figure 4b reveals that the surface slippage distresses the fluid temperature inversely by intensifying the slip parameter, the temperature profile boosts up and improves the thickness of the thermal boundary layer. It is also revealed that the velocity profile is marginally high for the kerosene-based magnetite (Fe_3O_4) nanofluid rather than for other fluids, although the temperature attains the highest increment in the Fe_3O_4–Refrigerant-134a-based nanofluid trailed by Fe_3O_4–water and Fe_3O_4–kerosene nanofluids.

Figure 5 demonstrates the influence of the suction parameter S = 0.0, 0.4, and 0.8 on the velocity profile for three dissimilar conventional fluids like kerosene ($C_{10}H_{22}$), water (H_2O), and Refrigerant-134a ($C_2H_2F_4$). It is confirmed that the velocity and associated momentum boundary layer thickness reduce against the suction parameter ($S > 0$).

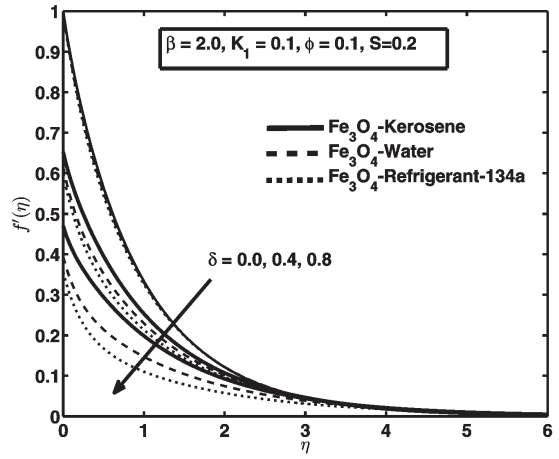

(a)

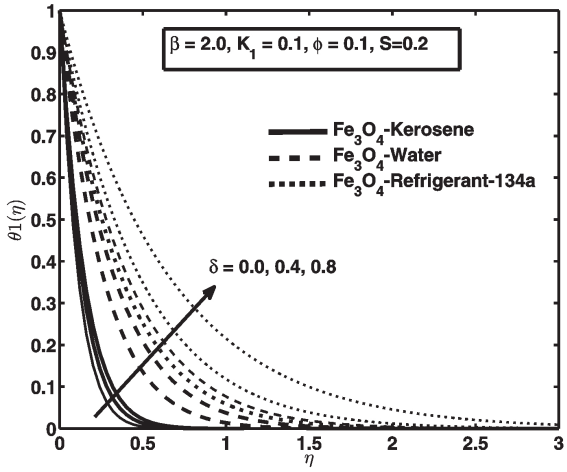

(b)

FIG. 4: (a) Sketch of δ on f', (b) sketch of δ on θ_1

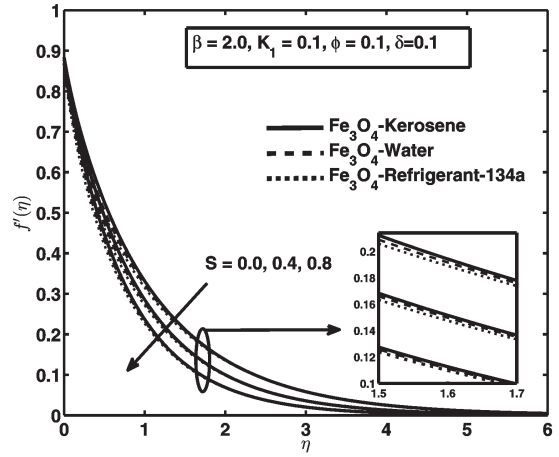

FIG. 5: Sketch of S on f'

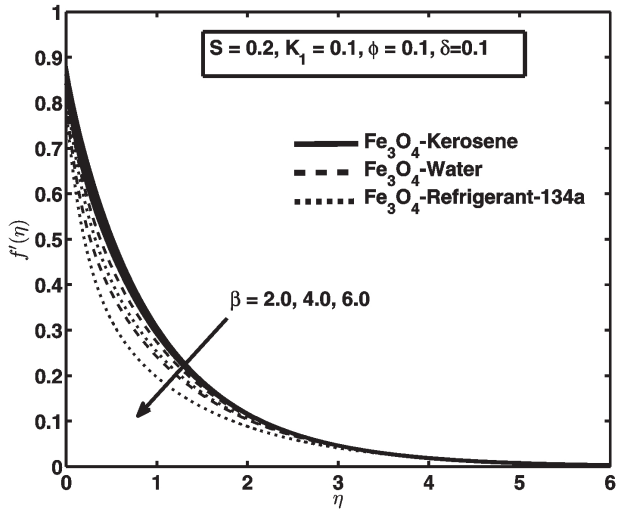

(a)

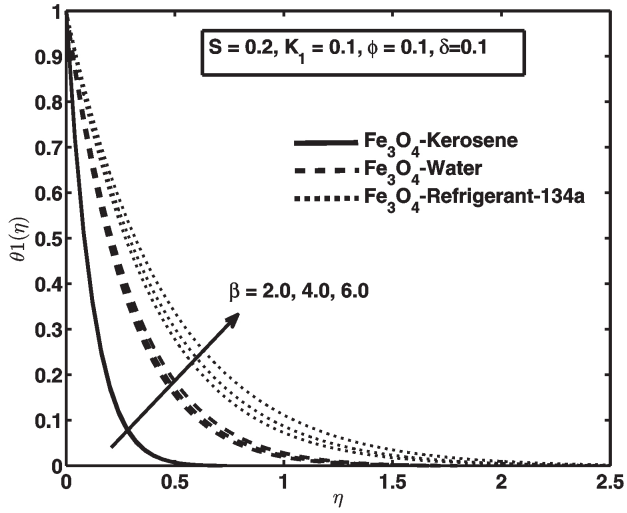

(b)

FIG. 6: (a) Sketch of β on f', (b) sketch of β on θ_1

Figure 6 exhibits the effect of the ferrohydrodynamic parameter β on the flow velocity and temperature profiles for three types of conventional liquids like kerosene ($C_{10}H_{22}$), Refrigerant-134a ($C_2H_2F_4$), and water (H_2O). The existence of dipole field plays as a delaying force having an ability to slow down the fluid motion; consequently, the higher value of β enhances the retarding force, therefore flattening the velocity field as shown in Fig. 6a, because there is collaboration between the fluid layers and the impact of an external magnetic field. This relation slows down the velocity field and enhances the frictional heating which is responsible for the increment in heat transfer as shown in Fig. 6b. Moreover it was observed that an increasing impact of temperature in magnetite (Fe_3O_4) based on Refrigerant-134a is more visible as compared to other.

Figure 7a clarifies the impact of the slip parameter δ on the skin friction for dissimilar conventional fluids with the addition of magnetite nanoparticles. The corresponding results examplify that the skin friction increases at a large value of volume fraction ϕ and a reducing effect is noted for slip. Also it was shown that the skin friction determines the utmost increment in the Fe_3O_4–Refrigerant-134a nanofluid as compared to others. This happens because of the lower Pr and C_p values of Refrigerant-134a rather than of kerosene and water.

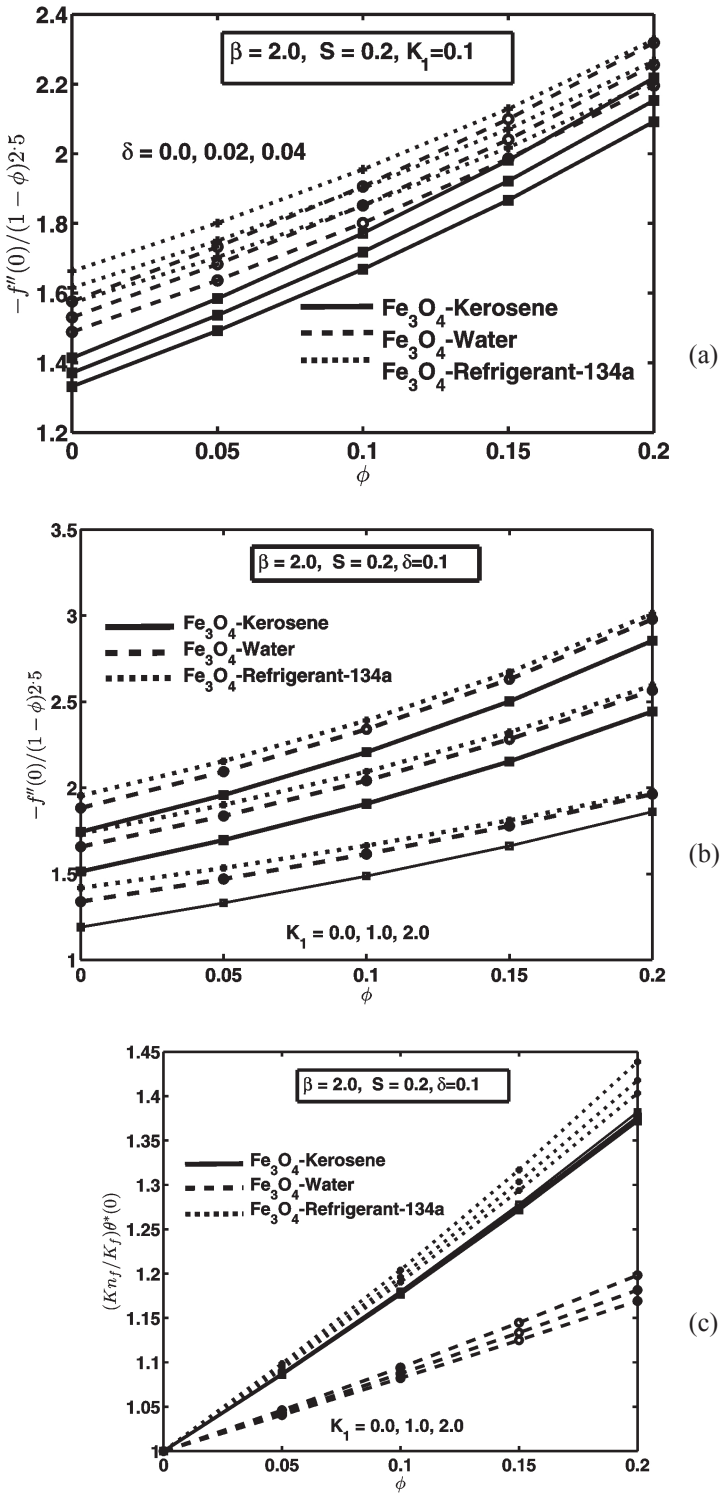

FIG. 7: (a) Sketch of δ on the skin friction coefficient vs. ϕ, (b) sketch of K_1 on the skin friction coefficient vs. ϕ, (c) sketch of K_1 on the Nusselt number vs. ϕ

TABLE 1: Thermophysical properties of base fluids and magnetite nanoparticles (Rosensweig, 2002; Oztop and Abu-Nada, 2008; Tillner-Roth and Baehr, 1992)

Physical Properties	Base Fluids			Magnetite Nanoparticles
	Water	Kerosene	Refrigerant-134a	Fe_3O_4
ρ, kg/m^3	997	783	1199.7	5180
c_p, J/(kg·K)	4179	2090	1432.0	670
k, W/m·K	0.613	0.15	0.0803	9.7
Pr	6.2	21	3.4	—

TABLE 2: Comparison of local Nusselt number for pure fluid at $\beta = \lambda = \phi = \delta = K_1 = S = 0$

Pr	Chen (1998)	Abel et al. (2008)	Gireesha et al. (2014)	Present Results
0.72	1.0885	1.0885	1.0885	1.088527
1	1.3333	1.3333	1.3333	1.333333
3	2.5097	—	2.5097	2.509725
10	4.7968	4.7968	4.7968	4.796873

TABLE 3: The calculated values of skin friction coefficient $C_f \mathrm{Re}_x^{1/2}$ and Nusselt number $\mathrm{Nu}_x \mathrm{Re}_x^{-1/2}$ at $K_1 = \delta = 0.1$, $S = 0.2$

—	ϕ	Magnetite Fe_3O_4 Nanoparticles					
		With the Ferromagnetic Interaction Parameter β = 2			Without the Ferromagnetic Interaction Parameter β = 2		
		Water Base	Kerosene Base	Refrigerant-134a Base	Water Base	Kerosene Base	Refrigerant-134a Base
$C_f \mathrm{Re}_x^{1/2}$	0.02	1.4489	1.3099	1.5189	1.0606	1.0727	1.0531
	0.05	1.5593	1.4336	1.6154	1.1626	1.1921	1.1440
	0.1	1.7563	1.6523	1.7895	1.3454	1.4032	1.3083
$\mathrm{Nu}_x \mathrm{Re}_x^{-1/2}$	0.02	0.2647	0.1183	0.3896	0.2565	0.1169	0.3718
	0.05	0.2991	0.1333	0.4385	0.2902	0.1317	0.4194
	0.1	0.3643	0.1614	0.5302	0.3540	0.1596	0.5091

Figure 7b portrays the porosity parameter K_1 impact on the skin friction for numerous values of nanoparticle volume fraction ϕ. The results reveal that the skin friction increases against the volume fraction and porosity parameter. The graph witnessed that the Fe_3O_4–kerosene-based nanofluid gains the lowest values as compared to remaining ones.

Figure 7c illustrates the effect of the porosity parameter K_1 on the heat transfer rate with the variation of solid volume fraction ϕ of magnetic nanoparticles. The graph shows an increasing effect of Nusselt number by varying the volume fraction, and the opposite behavior is observed for K_1. It is also noticed that the heat transfer rate for the Refrigerant-134a-based magnetic nanofluid obtained a maximum value rather than other cases. This is due to the fact that conventional Refrigerant-134a itself has a larger thermal conductivity when compared with different types of base liquid such as water and kerosene.

5. CLOSING REMARKS

We have examined heat transfer performance of ferrofluid flow via porous media with slip impact. We considered Refrigerant-134a ($C_2H_2F_4$), kerosene ($C_{10}H_{22}$), and water (H_2O) as a base fluid along with magnetite (Fe_3O_4) nanoparticles. The modeled governing flow problem is first converted into a set of ordinary differential equations applying appropriate similarity approach, and then elucidated by utilizing a shooting algorithm. Effects of various constraints like the ferromagnetic parameter β, slip parameter δ, porosity parameter K_1, suction parameter S, and the concentration of nanoparticles ϕ on the velocity field, temperature field, skin friction, and the Nusselt number are shown via graphs. Some major observations are in compact form as follows:

- By rising the volume fraction of nanoparticles, the porosity parameter, and the slip parameter, the fluid temperature increases, while the velocity profile decreases by increasing the ferromagnetic parameter β.
- The Fe_3O_4–Refrigerant-134a-based magnetic nanofluid obtained a higher temperature profile, followed by Fe_3O_4–kerosene and Fe_3O_4–water nanofluids.
- On increasing the concentration of nanoparticles, the skin friction rises, whereas it reduces against the slip parameter. The Fe_3O_4–Refrigerant-134a-based nanofluid reached the highest values as compared to kerosene- and water-based nanofluids.
- The Nusselt number has a maximum value in the case of the Fe_3O_4–Refrigerant-134a-based nanofluid than in the remaining base fluids with the variation of ϕ, due to the highest thermal conductivity of Refrigerant-134a.

REFERENCES

Abel, M.S., Sanjayanand, E., and Nandeppanavar, M.M., Viscoelastic MHD Flow and Heat Transfer over a Stretching Sheet with Viscous and Ohmic Dissipations, *Commun. Nonlinear Sci. Numer. Simul.*, vol. **13**, no. 9, pp. 1808–1821, 2008.

Andersson, H.I. and Valnes, O.A., Flow of a Heated Ferrofluid over a Stretching Sheet in the Presence of a Magnetic Dipole, *Acta Mech.*, vol. **128**, nos. 1–2, pp. 39–47, 1998.

Bhaskar R.N., Poornima, T., and Sreenivasulu, P., Influence of Variable Thermal Conductivity on MHD Boundary Layer Slip Flow of Ethylene-Glycol Based Cu Nanofluids over a Stretching Sheet with Convective Boundary Condition, *Int. J. Eng. Math*., vol. **2014**, Article ID 905158, pp. 1–10, 2014.

Bhatti, M.M. and Lu, D.Q., Analytical Study of the Head-On Collision Process between Hydroelastic Solitary Waves in the Presence of a Uniform Current, *Symmetry*, vol. **11**, no. 3, p. 333, 2019.

Chamkha, A.J. and Aly, A.M., MHD Free Convection Flow of a Nanofluid Past a Vertical Plate in the Presence of Heat Generation or Absorption Effects, *Chem. Eng. Commun*., vol. **198**, no. 3, pp. 425–441, 2010.

Chen, C.H., Laminar Mixed Convection Adjacent to Vertical, Continuously Stretching Sheets, *Heat Mass Transf*., vol. **33**, nos. 5–6, pp. 471–476, 1998.

Choi, S.U.S., Zhang, Z.G., Keblinski, P., and Nalwa, H.S., Nanofluids, in *Encyclopedia of Nanoscience and Nanotechnology*, Los Angeles, CA: American Scientific Publishers, pp. 757–737, 2004.

Choi, S.U.S., Enhancing Thermal Conductivity of Fluids with Nanoparticles, in *Developments and Applications of Non-Newtonian Flows*, D.A. Signer and H.P. Wang, Eds., vol. **66**, pp. 99–105, New York: ASME, 1995.

Ellahi, R., Bhatti, M.M., and Vafai, K., Effects of Heat and Mass Transfer on Peristaltic Flow in a Non-Uniform Rectangular Duct, *Int. J. Heat Mass Transf*., vol. **71**, pp. 706–719, 2014.

Ellahi, R., Hassan, M., and Zeeshan, A., Shape Effects of Nanosize Particles in Cu–H_2O Nanofluid on Entropy Generation, *Int. J. Heat Mass Transf.*, vol. **81**, pp. 449–456, 2015.

Gireesha, B.J., Mahanthesh, B., and Gorla, R.S.R., Suspended Particle Effect on Nanofluid Boundary Layer Flow past a Stretching Surface*, J. Nanofluids*, vol. **3**, no. 3, pp. 267–277, 2014.

Hassan, M., Ellahi, R., Zeeshan, A., and Bhatti, M.M., Analysis of Natural Convective Flow of Non-Newtonian Fluid under the Effects of Nanoparticles of Different Materials, *P. I. Mech. Eng. E-J Pro.*, vol. **233**, no. 3, pp. 643–652, 2019.

Hassan, M., Marin, M., Alsharif, A., and Ellahi, R., Convective Heat Transfer Flow of Nanofluid in a Porous Medium over Wavy Surface, *Phys. Lett. A*, vol. **382**, no. 38, pp. 2749–2753, 2018.

Kefayati, G.H.R., Natural Convection of Ferrofluid in a Linearly Heated Cavity Utilizing LBM, *J. Mol. Liq.*, vol. **191**, pp. 1–9, 2014.

Khan, W.A. and Pop, I., Free Convection Boundary Layer Flow Past a Horizontal Flat Plate Embedded in a Porous Medium Filled with a Nanofluid*, J. Heat Transf.*, vol. **133**, no. 9, p. 094501, 2011.

Kumar, D.S. and Elansezhian, R., Experimental Study on Al_2O_3–R134a Nano Refrigerant in Refrigeration System, *Int. J. Modern Eng. Res*., vol. **2**, no.5, pp. 3927–3929, 2012.

Lee, S., Choi, S.U.S., Li, S.A., and Eastman, J.A., Measuring Thermal Conductivity of Fluids Containing Oxide Nanoparticles, *J. Heat Transf.,* vol. **121**, no. 2, pp. 280–289, 1999.

Majeed, A., Zeeshan, A., and Gorla, R.S.R., Convective Heat Transfer in a Dusty Ferromagnetic Fluid over a Stretching Surface with Prescribed Surface Temperature/Heat Flux Including Heat Source/Sink, *J. Natl. Sci. Found. Sri Lanka,* vol. **46**, no. 3, 2018.

Majeed, A., Zeeshan, A., and Hayat, T., Analysis of Magnetic Properties of Nanoparticles due to Applied Magnetic Dipole in Aqueous Medium with Momentum Slip Condition, *Neural Comput. Appl*., vol. **31**, no. 1, pp. 189–197, 2019a.

Majeed, A., Zeeshan, A., and Noori, F.M., Numerical Study of Darcy-Forchheimer Model with Activation Energy Subject to Chemically Reactive Species and Momentum Slip of Order Two, *AIP Adv.*, vol. **9**, no. 4, p. 045035, 2019b.

Majeed, A., Zeeshan, A., Mahmood, T., Rahman, S.U., and Khan, I., Impact of Magnetic Field and Second-Order Slip Flow of Casson Liquid with Heat Transfer Subject to Suction/Injection and Convective Boundary Condition, *J. Magn*., vol. **24**, no. 1, pp. 81–89, 2019c.

Mamourian, M., Shirvan, K.M., Ellahi, R., and Rahimi, A.B., Optimization of Mixed Convection Heat Transfer with Entropy Generation in a Wavy Surface Square Lid-Driven Cavity by Means of Taguchi Approach, *Int. J. Heat Mass Transf*., vol. **102**, pp. 544–554, 2016.

Marin, M. and Öchsner, A., The Effect of a Dipolar Structure on the Hölder Stability in Green–Naghdi Thermoelasticity, *Continuum Mech. Therm.,* vol. **29**, no. 6, pp. 1365–1374, 2017.

Masuda, H., Ebata, A., and Teramae, K., Alteration of Thermal Conductivity and Viscosity o Liquid by Dispersing Ultra-Fine Particles. Dispersion of Al_2O_3, SiO_2 and TiO_2 Ultra-Fine Particles, *Netsu Bussei.,* vol. **7**, no. 227, pp. 227–233, 1993.

Mohyud-Din, S.T., Zaidi, Z.A., Khan, U., and Ahmed, N., On Heat and Mass Transfer Analysis for the Flow of a Nanofluid between Rotating Parallel Plates, *Aerosp. Sci. Technol*., vol. **46**, pp. 514–522, 2015.

Nadeem, S., Mehmood, R., and Akbar, N.S., Non-Orthogonal Stagnation Point Flow of a Nano Non-Newtonian Fluid towards a Stretching Surface with Heat Transfer, *Int. J. Heat Mass Transf*., vol. **57**, no. 2, pp. 679–689, 2013.

Oztop, H.F. and Abu-Nada, E., Numerical Study of Natural Convection in Partially Heated Rectangular Enclosures Filled with Nanofluids, *Int. J. Heat Fluid Flow*, vol. **29**, no. 5, pp. 1326–1336, 2008.

Rahman, M.M., Al-Lawatia, M.A., Eltayeb, I.A., and Al-Salti, N., Hydromagnetic Slip Flow of Water Based Nanofluids Past a Wedge with Convective Surface in the Presence of Heat Generation (or) Absorption, *Int. J. Therm. Sci*., vol. **57**, pp. 172–182, 2012.

Rajesh, V., Mallesh, M.P., and Bég, O.A., Transient MHD Free Convection Flow and Heat Transfer of Nanofluid Past an Impulsively Started Vertical Porous Plate in the Presence of Viscous Dissipation, *Procedia Mater. Sci*., vol. **10**, pp. 80–89, 2015.

Reddy, P.S. and Chamkha, A.J., Influence of Size, Shape, Type of Nanoparticles, Type and Temperature of the Base Fluid on Natural Convection MHD of Nanofluids, *Alexandria Eng. J*., vol. **55**, no. 1, pp. 331–341, 2016.

Rosensweig, R.E., Heating Magnetic Fluid with Alternating Magnetic Field, *J. Magn. Magn. Mater*, vol. **252**, pp. 370–374, 2002.

Sheikholeslami, M. and Ellahi, R., Three-Dimensional Mesoscopic Simulation of Magnetic Field Effect on Natural Convection of Nanofluid, *Int. J. Heat Mass Transf*., vol. **89**, pp. 799–808, 2015.

Sheikholeslami, M. and Ganji, D.D., Ferrohydrodynamic and Magnetohydrodynamic Effects on Ferrofluid Flow and Convective Heat Transfer, *Energy*, vol. **75**, pp. 400–410, 2014.

Sheikholeslami, M. and Rashidi, M.M., Effect of Space Dependent Magnetic Field on Free Convection of Fe_3O_4–Water Nanofluid, *J. Taiwan Inst. Chem. Eng*., vol. **56**, pp. 6–15, 2015.

Sheikholeslami, M., Ellahi, R., Shafee, A., and Li, Z., Numerical Investigation for Second Law Analysis of Ferrofluid Inside a Porous Semi Annulus: An Application of Entropy Generation and Exergy Loss, *Int. J. Numer. Method H.*, vol. **29***,* no. 3, pp. 1079–1102, 2019.

Sheikholeslami, M., Ganji, D.D., and Rashidi, M.M., Ferrofluid Flow and Heat Transfer in a Semi Annulus Enclosure in the Presence of Magnetic Source Considering Thermal Radiation, *J. Taiwan Inst. Chem. Eng*., vol. **47**, pp. 6–17, 2015a.

Sheikholeslami, M., Rashidi, M.M., and Ganji, D.D., Effect of Non-Uniform Magnetic Field on Forced Convection Heat Transfer of Fe_3O_4–Water Nanofluid, *Comput. Method Appl. M*, vol. **294**, pp. 299–312, 2015b.

Sheikholeslami, M., Zeeshan, A., and Majeed, A., Control Volume Based Finite Element Simulation of Magnetic Nanofluid Flow and Heat Transport in Non-Darcy Medium, *J. Mol. Liq.*, vol. **268**, pp. 354–364, 2018.

Tillner-Roth, R. and Baehr, H.D., Burnett Measurements and Correlation of Gas-Phase (P, P, T) of 1,1,1,2-Tetrafluoroethane (R 134a) and of 1,1-Difluoroethane (R 152a), *J. Chem. Thermodyn.*, vol. **24**, no. 4, pp. 413–424, 1992.

Tiwari, R.K. and Das, M.K., Heat Transfer Augmentation in a Two-Sided Lid-Driven Differentially Heated Square Cavity Utilizing Nanofluids, *Int. J. Heat Mass Transf.*, vol. **50**, nos. 9–10, pp. 2002–2018, 2007.

Yirga, Y. and Tesfay, D., Heat and Mass Transfer in MHD Flow of Nanofluids through a Porous Media Due to a Permeable Stretching Sheet with Viscous Dissipation and Chemical Reaction Effects, *Int. J. Mech. Aero. Indus. Mech. Manu. Eng*., vol. **9**, pp. 674–681, 2015.

Yu, W., France, D.M., Routbort, J.L., and Choi, S.U., Review and Comparison of Nanofluid Thermal Conductivity and Heat Transfer Enhancements, *Heat Transf. Eng*., vol. **29**, no. 5, pp. 432–460, 2008.

Zeeshan, A., Majeed, A., Ellahi, R., and Zia, Q.M.Z., Mixed Convection Flow and Heat Transfer in Ferromagnetic Fluid over a Stretching Sheet with Partial Slip Effects, *J. Therm. Sci*., vol. **22**, no. 6, pp. 2515–2526, 2018.